The Steady-State Barotropic Response of the Gulf of Maine and Adjacent Regions to Surface Wind Stress

DANIEL G. WRIGHT, DAVID A. GREENBERG, JOHN W. LODER AND PETER C. SMITH

Atlantic Oceanographic Laboratory, Department of Fisheries and Oceans, Bedford Institute of Oceanography, Dartmouth, N.S., Canada B2Y 4A2

(Manuscript received 9 July 1985, in final form 4 December 1985)

ABSTRACT

The response of the Gulf of Maine region to steady, spatially uniform wind stress is examined using a linearized numerical model, with the influence of the strong tidal currents in the region included in the bottom stress formulation. The sensitivity of the model results to various idealizations is investigated, including the assumption of linearity, the bottom stress formulation, cross-shelf structure in the (large-scale) alongshelf wind stress and the cross-shelf boundary conditions. The model solutions for the Gulf are found to be sensitive to the "backward" boundary condition on the Scotian Shelf, but not to the "forward" boundary condition in the Middle Atlantic Bight. For alongshelf stress, the former is estimated using Csanady's "arrested topographic wave" model and observed coastal sea level gains at Halifax.

The model has a spinup time of about one day, comparable to previous estimates for the region. The alongshelf component of wind stress is generally much more effective than the cross-shelf component in driving currents and sea level changes in the model. The predicted large-scale circulation features and coastal sea level changes compare favorably with those observed, and there is reasonable agreement between predicted and observed currents off southwestern Nova Scotia for alongshelf stress. The dynamics of the model response are discussed in terms of the arrested topographic wave model and Ekman dynamics, and using the momentum balances at some current meter observation sites.

1. Introduction

The Gulf of Maine (GOM) is a major feature of the eastern North American continental shelf, extending about 400 km in the alongshelf direction and forming an approximately 150 km indentation of the coastline (Fig. 1). The irregular bottom topography of the region is dominated by several large deep basins in the GOM itself and by a series of submarine banks along the outer shelf which form a partial obstruction to exchange with the deep ocean. The primary deep link between the GOM's basins and adjacent regions is the Northeast Channel separating Georges and Browns Banks. To the east, in the "backward" direction for continental shelf wave propagation, the GOM merges with the rugged Scotian Shelf (SS) which extends a distance of about 600 km along the coast of Nova Scotia to the Laurentian Channel running seaward from Cabot Strait. In the "forward" direction to the southwest, the GOM adjoins the topographically smoother Middle Atlantic Bight (MAB).

The residual (after the removal of tidal motions) circulation on the SS and in the MAB includes a net southwestward flow of 0.02–0.10 m s^{-1} (e.g., Smith et al., 1978; Beardsley and Boicourt, 1981) which is generally considered to continue through the GOM but with considerable spatial complexity. The main features of the residual circulation in the GOM region have been identified as an inflow off southwestern Nova Scotia (Smith, 1983), an outflow towards the southwest through Great South Channel (Butman et al., 1982) and across Nantucket Shoals (Beardsley et al., 1985), an inflow at depth through Northeast Channel (Ramp et al., 1986), anticyclonic gyres around Browns (Smith, 1983) and Georges Banks (Butman et al., 1982), and a cyclonic gyre in the inner GOM (Bigelow, 1927) with some recirculation over Jordan Basin (Brooks, 1985). Although the currents have varying degrees of vertical structure, it is generally considered that, with the exception of the Northeast Channel inflow, these features are present to some extent throughout the water column. On the other hand, considerable temporal variability in most of these circulation features has been observed, particularly with season (e.g., Smith, 1983; Butman et al., 1985) and on the time scales of atmospheric variability (e.g., Noble et al., 1983).

The dynamical origin of the circulation in the GOM region has been the subject of a large number of theoretical investigations during the past decade (e.g., Csanady, 1974, 1979; Loder, 1980; Shaw, 1982; Wang, 1982, 1984; Isaji et al., 1982; Brink, 1983; Greenberg, 1983; Smith, 1983; Loder and Wright, 1985). These investigations have suggested that there are significant contributions to the circulation from the rectification of tidal currents over the variable bottom topography, horizontal density gradients, externally imposed pres-

sure gradients and surface wind stress, the latter of which we examine here.

Observational evidence for a significant contribution from wind stress forcing to low-frequency current and sea level variability in the region has been presented by several investigators. Noble and Butman (1979) examined coastal sea level records from 14 locations in the GOM, on the SS and in the MAB for a 6-month period in 1973–74 and found variations with periods between 2.5 and 25 days associated with the alongshelf stress. Sandstrom (1980) found that subtidal sea level changes at Halifax and Yarmouth are highly correlated with the alongshelf stress (as well as wind velocity) even at periods exceeding 30 days, and Thompson (1986) has recently reported variations in monthly averaged values of sea level at Halifax and several GOM coastal sites which are correlated with low-frequency variations in both the alongshelf and cross-shelf stress estimated from atmospheric pressure maps. Noble et al. (1983) and Noble et al. (1985) analyzed current measurements from the open ocean side of Georges Bank and showed that a significant portion of the subtidal variability in alongshelf current, including variability at periods of up to 56 days, was directly associated with the alongshelf stress. Furthermore, there should be a significant contribution to the low-frequency circulation in the GOM from the strong seasonal variation in the region's stress field which has seasonal mean magnitudes ranging from about 0.02 Pa in summer to order 0.1 Pa in winter (Saunders, 1977).

Previous theoretical investigations of low-frequency wind stress forcing in the GOM region have included the idealized model studies of Csanady (1974), Shaw (1982) and Brink (1983), and the numerical model studies of Beardsley and Haidvogel (1981), Isaji et al. (1982) and Greenberg (1983). Beardsley and Haidvogel (1981) used a linear barotropic model to examine the transient response of the GOM and MAB to stress forcing, while Greenberg (1983) determined the residual circulation associated with Saunders' (1977) seasonal mean stresses using a nonlinear barotropic model. However, the residual elevation on all open boundaries in these models was fixed at zero, whereas Hayashi et al. (1986) have shown that such a condition on the cross-shelf boundaries may lead to poor results.

The purpose of this study is to complement earlier work with a numerical model investigation of the steady-state barotropic response of the region to steady surface wind stress. The emphases are on the appropriate boundary condition for the backward cross-shelf boundary on the SS, on determining the sensitivity of model results to various uncertainties and simplifications, and on relating model predictions to the observations of circulation and coastal sea level variability in the region. The results of the study should be relevant to the region's response to low-frequency wind stress patterns with periods much greater than the region's adjustment time scale (see section 4).

In section 2, the linearized numerical model used in the study is described, while in section 3, the choice of an appropriate backward boundary condition for the SS boundary is examined. The model results for steady, uniform wind stress in the alongshelf and cross-shelf directions are presented in section 4, and the sensitivity of the results to various simplifications are discussed in section 5. In section 6, the predicted gains in coastal sea level around the GOM and in currents off southwestern Nova Scotia are compared with observations, and in section 7, the predicted momentum balances at some current meter observation sites are discussed. Finally, results and conclusions are summarized in section 8.

2. The numerical model

Neglecting the nonlinear advective terms and assuming $\zeta \ll h$, the barotropic equations for nontidal (low-frequency) motion in a homogeneous, incompressible, hydrostatic fluid can be written as

$$\frac{\partial u}{\partial t} - fv = -g\frac{\partial \zeta}{\partial x} + \frac{\tau_x^s - \tau_x^b}{\rho h} \tag{1a}$$

$$\frac{\partial v}{\partial t} + fu = -g\frac{\partial \zeta}{\partial y} + \frac{\tau_y^s - \tau_y^b}{\rho h} \tag{1b}$$

$$\frac{\partial \zeta}{\partial t} + \frac{\partial}{\partial x}(hu) + \frac{\partial}{\partial y}(hv) = 0, \tag{2}$$

where

$$\frac{\tau_x^b}{\rho} = c_D\left(v_b + \frac{\overline{2U^2 + V^2}}{(U^2 + V^2)^{1/2}}\right)u + c_D\frac{\overline{UV}}{(U^2 + V^2)^{1/2}}v \tag{3a}$$

$$\frac{\tau_y^b}{\rho} = c_D\frac{\overline{UV}}{(U^2 + V^2)^{1/2}}u + c_D\left(v_b + \frac{\overline{U^2 + 2V^2}}{(U^2 + V^2)^{1/2}}\right)v. \tag{3b}$$

The notation in these equations is as follows:

t	time
x, y, z	a right-handed Cartesian coordinate system with x directed in the cross-shelf (positive offshore) direction, y in the alongshelf (backward) direction and z vertically upward with $z = 0$ corresponding to the position of the sea surface in the absence of motion
u, v	the x- and y-components of nontidal velocity
U, V	the x- and y-components of tidal velocity
v_b	the speed of other background currents (taken as 0.1 m s^{-1})
h	the water depth in the absence of motion
ζ	the surface elevation above $z = 0$
τ_x^s, τ_y^s	the x- and y-components of the surface stress
τ_x^b, τ_y^b	the x- and y-components of the bottom stress
f	the Coriolis parameter specified to vary with latitude

g the acceleration due to gravity
ρ the density of seawater (assumed constant)
c_D the drag coefficient in a quadratic bottom stress law (taken here as 2.3×10^{-3}).

Equations (3a), (3b), are time-averaged (indicated by an overbar), linearized approximations to a quadratic stress law of the form

$$(\tau_x^{b'}, \tau_y^{b'}) = \rho c_D[v_b + (u'^2 + v'^2)^{1/2}](u', v') \quad (4)$$

where (u', v') refer to the M_2-tidal plus steady wind-driven velocity components. They were derived following Heaps (1978) by time-averaging (4) under the assumption that the nontidal velocity is small compared to the tidal velocity. The parenthesized coefficients in (3a), (3b) are evaluated using the M_2 tidal velocities computed using another (tidal) version (Greenberg, 1983) of the present numerical model, and v_b is included in (4) to represent (crudely) the influence of other currents (e.g., other tidal constituents, tidally rectified mean currents and wind-driven currents) which are not explicitly included in our estimate of the background current field.

The high-resolution ($\approx$7 km) numerical model grid of Greenberg (1983) is used. The model domain (see Figs. 1 and 7) thus includes the entire GOM and over half of the Bay of Fundy, extending seaward to the shelf break and about 150 km onto the adjoining SS

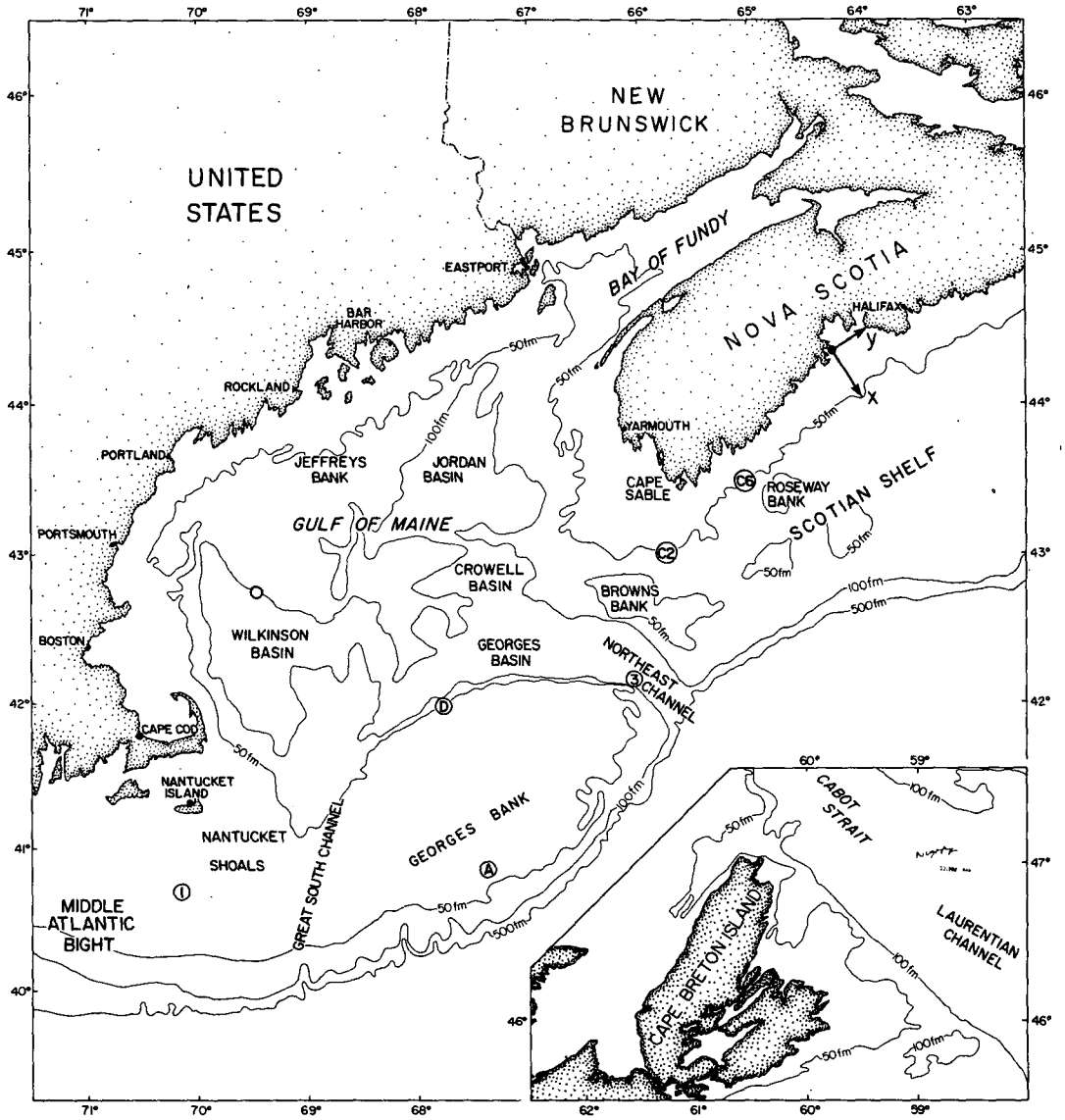

FIG. 1. Topographic map of the Gulf of Maine and adjacent regions showing the major features and observation sites referred to in the text. The orientation of the coordinate system used in the model is indicated. The x-axis marks the backward extent of the model domain.

and MAB. The equations of motion are discretized and solved as described by Greenberg (1983), with the exception of the conditions specified on the open boundaries. In Greenberg's (1983) simulations of the residual circulation in the GOM due to the seasonal mean wind stresses and tidal rectification, only oscillatory tidal elevations were specified on the open boundaries. In the present study, the conditions of zero residual elevation on the shelf-break boundary and zero flow normal to land boundaries are retained, but an alternative to the specification of zero residual elevation on the cross-shelf boundaries is used.

The prescription of zero elevation on the shelf-break boundary is consistent with the observational evidence described by Beardsley and Haidvogel (1981) for the adjusted surface elevation over the adjacent continental slope and deep ocean being constant to within ±1 cm, and with the theoretical result (Shaw, 1982; Wang, 1982; Brink, 1983) that, in a barotropic fluid, the continental slope effectively insulates the shelf from the influence of low-frequency circulation in the deep ocean. Also, if low-frequency elevation variations at the shelf-break were allowed to be of the same order of magnitude (0.1 m) as those observed at the coast, then the abrupt reduction in elevation across the continental slope would imply unreasonably large geostrophic transports along the slope.

At the cross-shelf boundaries on the SS and in the MAB, we use the radiation boundary condition

$$v - v_0 = \pm\left(\frac{g}{h}\right)^{1/2}(\zeta - \zeta_0), \tag{5}$$

where v_0 and ζ_0 are prescribed estimates of alongshelf velocity and elevation on the boundary, and the positive (negative) sign corresponds to the SS (MAB) boundary. Deviations from v_0 and ζ_0 are thus assumed to be outwardly propagating (from the model domain) gravity waves. Note, however, that (5) also allows the development along the cross-shelf boundaries of an additional geostrophically balanced mean elevation field which satisfies

$$\frac{\partial \zeta_g}{\partial x} = -R_e^{-1}\zeta_g, \tag{6}$$

where $R_e (\equiv (gh)^{1/2}/f)$ is the local external Rossby radius of deformation.

The values of v_0 and ζ_0 in (5) can be specified to be consistent with observations and theoretical models of wind-driven circulation on the SS and in the MAB. In this study, we follow the conceptual framework of Csanady's (1978) "arrested topographic wave" model (ATWM), which predicts that the effects of wind stress are only felt over the portion of the shelf towards which continental shelf waves propagate. The expected insensitivity of the model results to the values of v_0 and ζ_0 on the MAB boundary is confirmed by numerical model runs (see section 5b), so we simply specify v_0 and ζ_0 to be zero on this boundary. However, as discussed in the next section, the specification of reasonable values for v_0 and ζ_0 on the SS boundary is more critical.

The remaining open boundary in the model is across the upper Bay of Fundy. Since we expect the net transport into the upper Bay to be zero in the steady states that are of interest here, we uniformly adjust the elevations on this boundary to satisfy this constraint.

3. The backward boundary condition

Under the assumption of linearity, the response of the GOM to steady, spatially uniform wind stress can be examined by determining its response to wind stress of unit magnitude in two perpendicular directions—taken here as the large-scale alongshelf (+y; 56°T) and cross-shelf (+x; 146°T) directions.

a. Alongshelf wind stress

The possible significance of the backward boundary condition is illustrated by a comparison of the theoretical prediction for alongshelf wind stress forcing under the assumption of uniformity in the alongshelf direction with observations of coastal sea level gain (per unit forcing) at Halifax (situated near the numerical model's backward boundary). For steady motion in the "infinite shelf model" (ISM), the sea level elevation at the coast ($x = 0$) is given by (e.g., Hayashi et al., 1986)

$$\zeta(0) = -L_w\left(\frac{f\tau_y^s}{\rho g k}\right), \tag{7}$$

where L_w is the shelf width and the linear bottom stress law $\tau_y^b = \rho k v$ has been used. From (3b) we estimate the value of the (constant) linear friction coefficient k to be in the range of $(2.5\text{–}7.5) \times 10^{-4}$ m s^{-1} on the SS. Then with the shelf width taken as 200 km, this simple model predicts that a 0.1-Pa alongshelf wind stress over the SS should result in a coastal sea level setdown in the range of 0.27 to 0.82 m. Furthermore, the wind-driven transport along the shelf is predicted to be

$$T = \int_0^{L_w} hv\,dx = A\left(\frac{\tau_y^s}{\rho k}\right), \tag{8}$$

which yields a northeastward transport in the range of $(3.7\text{–}11.0) \times 10^6$ m^3 s^{-1} on the SS (cross-sectional area $A \approx 2.8 \times 10^7$ m^2) for each 0.1 Pa of stress.

However, comparison of this estimate of sea level gain with the observed gains reported by Noble and Butman (1979), Sandstrom (1980) and Thompson (1986) suggests that the ISM significantly overestimates the response of the SS to alongshelf wind stress. Noble and Butman's (1979) analysis of adjusted sea level at Halifax reveals an average gain of -1.1 m Pa^{-1} for alongshelf stress in winter, assuming a surface drag coefficient of 1.6×10^{-3}. Sandstrom's (1980) results

indicate that, in the lowest frequency band (0–0.05 cpd), the sea level gain at Halifax is approximately −0.9 m Pa^{-1} for alongshelf stress in both winter and summer. (This gain is calculated by converting Sandstrom's unit wind velocity to wind stress using Wright and Thompson's (1983) linearized approximation to the quadratic surface stress law and Thompson and Hazen's (1983) values of 8.0 and 4.8 m s^{-1} for the standard deviation of high-frequency wind speed fluctuations over the SS in winter and summer respectively.) Furthermore, K. R. Thompson (private communication, 1985; also see Thompson, 1986) has examined sea level variability in the period range of 2–72 mo and found a gain at Halifax of about −0.3 m Pa^{-1} for alongshelf stress over the SS. These gains are all substantially smaller in magnitude than those predicted by the ISM (2.7–8.2 m Pa^{-1}) and indicate that, although the frequency-dependence of the sea level response may be reproduced by the ISM (Sandstrom, 1980), the magnitude of the response is not predicted accurately. The discrepancy among the observed gains is apparently due to a combination of Noble and Butman's (1979) and Sandstrom's (1980) use of wind velocity observations from Halifax which are lower than those over the SS (e.g., Saunders, 1977), the different frequency ranges of the gains, and uncertainty in Thompson's (1986) estimation of surface wind stress from geostrophic wind velocity (see section 6 for further discussion of these observed gains).

The inadequacy of the ISM as a dynamical approximation to the SS is not surprising in light of the theoretical guidance provided by the ATWM (Csanady, 1978). The ATWM suggests that the coastal sea level response on the SS boundary may be limited by both the finite horizontal scale of the stress field and the finite extent of the backward portion of the SS. For example, the coastal barrier appears to extend only about 350 km to the northeast, at which point Cabot Strait should permit a relatively unobstructed Ekman transport. Csanady's (1978) solution for uniform wind stress along only part of an infinite plane-beach shelf predicts an elevation field which is trapped against the coast with a cross-shelf decay scale

$$L_x(-y) \equiv -\zeta(\partial\zeta/\partial x)^{-1}|_{x=0} = \left(-\frac{4ky}{\pi fs}\right)^{1/2}, \quad (9)$$

where $-y$ is the distance from the shelf's backward origin and s is the (constant) cross-shelf bottom slope. The corrected version (Winant, 1979) of Csanady's (1978) formula (24) predicts that the coastal sea level is

$$\zeta(0, -y) = -\left(-\frac{4ky}{\pi fs}\right)^{1/2}\left(\frac{f\tau_y^s}{\rho gk}\right) = -L_x\left(\frac{f\tau_y^s}{\rho gk}\right), \quad (10)$$

and the alongshelf transport is

$$T(-y) = -\left(\frac{\tau_y^s}{\rho f}\right)y = \frac{\pi}{2}A'\left(\frac{\tau_y^s}{\rho k}\right), \quad (11)$$

where $A'(-y)$ $(=sL_x^2/2)$ is the cross-sectional area within the decay scale L_x [given by (9)] of the coast. Comparison of (10) and (11) with (7) and (8) indicates that the finite backward extent of the shelf reduces the coastal sea level gain and the alongshelf transport on a plane-beach shelf by the factors $L_x/L_w[\propto(-y)^{1/2}]$ and $\pi A'/(2A)[\alpha(-y)]$, respectively. With k and s in the ranges of (2.5–7.5) × 10^{-4} m s^{-1} and (1–2) × 10^{-3}, appropriate to the SS, the cross-shelf decay scale and coastal sea level gain at the backward boundary of our model domain ($-y$ = 350 km) are predicted to be in the ranges of (24–58) km and −(0.56–1.4) m Pa^{-1} respectively, and the transport across the boundary for a 0.1 Pa stress is only 3.5 × 10^5 m^3 s^{-1}.

Considering the observed gains and the ATWM results, in our base case for alongshelf stress we approximate ζ_0 on the SS boundary by a setup/setdown of 0.1 m at the coast for each 0.1 Pa of stress and an exponential decrease offshore with a decay scale of 39 km, and specify v_0 consistent with a cross-shelf geostrophic balance. The value of the cross-shelf decay scale is consistent with (9) for uniform stress along part of a plane-beach shelf with k = 5.0 × 10^{-4} m s^{-1}, s = 1.5 × 10^{-3} and $-y$ = 350 km. The results with this boundary condition, henceforth referred to as a 0.1 m exponential setup/setdown, can then be compared with those using other boundary specifications and with observed sea levels and currents (section 6) to provide further insight into the appropriate backward boundary condition (indeed, the results in section 6 suggest that a 0.05 m coastal setup/setdown with a linear decrease offshore may be more appropriate although there are only minor differences in the model predictions for the GOM which is of primary interest here).

Figure 2 shows the predicted elevations and (depth-averaged) currents for the GOM region with this 0.1 m exponential setup on the SS boundary as the only forcing in the numerical model, i.e., with τ_x^s, τ_y^s = 0 over the model domain and ζ_0, v_0 = 0 on the MAB boundary. Note that, through the radiation condition (5), there is some adjustment of the computed elevations and velocities on the MAB and SS boundaries away from the specified values of ζ_0 and v_0, reflecting the complexity of the topography in the vicinity of the boundaries. Nevertheless, the predictions can be considered to be estimates of the result of either a spatially uniform, −0.1 Pa alongshelf wind stress over the backward (outside the model domain) portion of the SS, or a southwestward barotropic transport of unspecified dynamical origin and magnitude approximately 7 × 10^5 m^3 s^{-1} across the SS boundary (comparable to the wintertime geostrophic transport estimated by Drinkwater et al., 1979, for the Halifax section). With the present assumption of linearity, the sign and direction of the elevations and velocities in Fig. 2 are simply reversed with the sign of the alongshelf wind stress or transport. The sensitivity to the detailed form of ζ_0, v_0 on the SS and MAB boundaries is discussed in sections 5a, b.

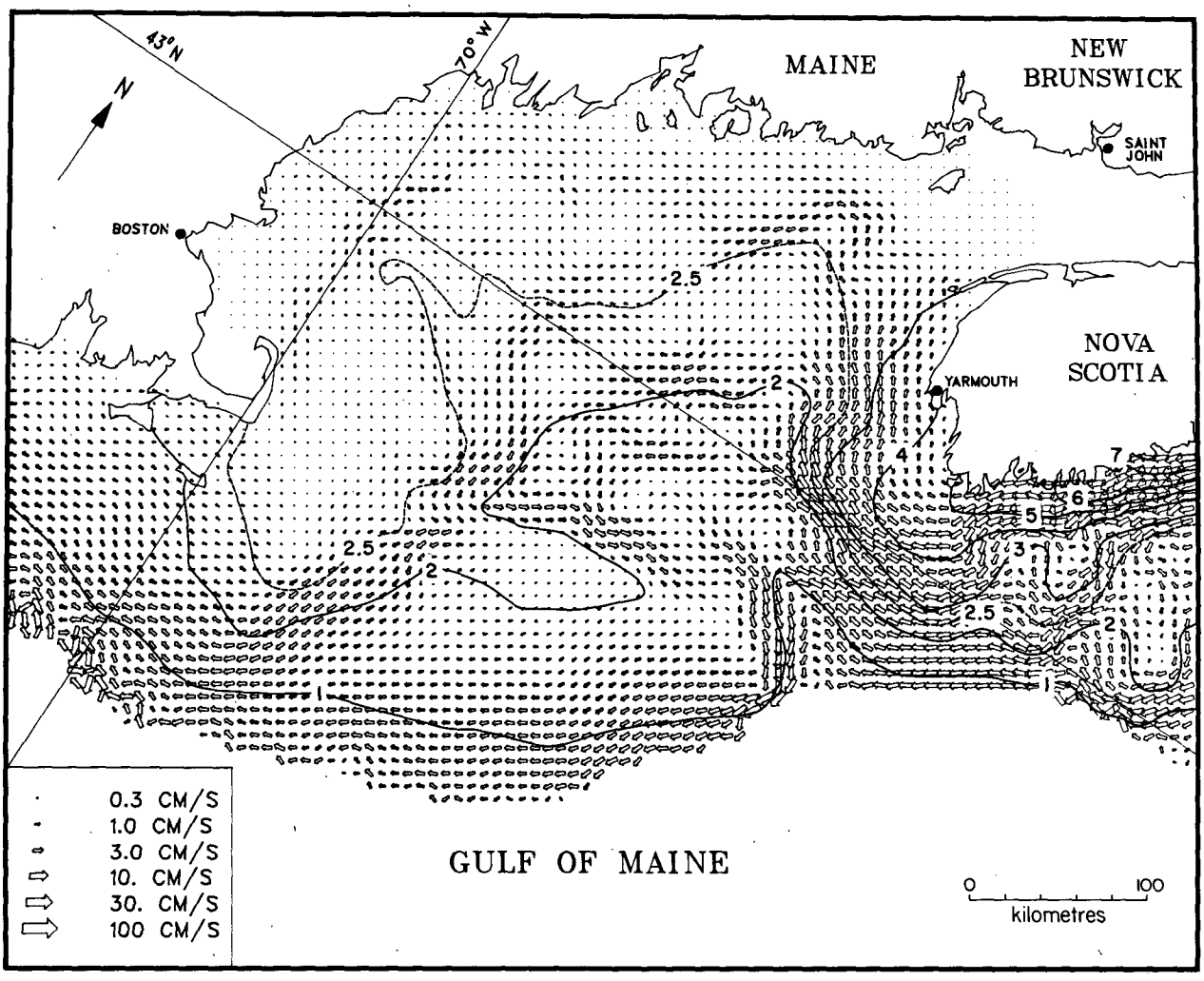

FIG. 2. Predicted elevations (cm) and currents for a 0.1 m exponential setup across the backward boundary of the numerical model and no wind stress over the model domain. The large currents near the shelf edge here and in Figs. 4, 5 and 6 are an artifact resulting from the numerical scheme, boundary conditions and steep topography, and have a negligible influence on the results discussed in this paper.

The numerical model solution (Fig. 2) has some of the gross features expected from the idealized ATWM, but also indicates a strong influence from the pronounced topographic variations in the region. The surface elevation decays away from the specified setup on the SS boundary such that there is a setup of 0.02–0.03 m over much of the GOM, and of 0.01–0.02 m over the inner MAB. The 0.1–0.2 m s^{-1} inflow across the SS boundary within about 40 km of the coast broadens to a southwestward flow of about 0.05 m s^{-1} across the entire shelf in the Cape Sable region. This broadening is much more abrupt than in the idealized solutions, apparently due to the influence of topographic features such as Roseway Bank. There is also a small contribution to the transport in the Cape Sable region from the inflow across the outer portion of the SS boundary allowed by the radiation condition, but the current pattern in this corner of the model domain may be merely an artifact of the irregular shelf-break boundary. In the GOM, a strong tendency for flow along geostrophic (f/h) contours is apparent, including a substantial deflection of flow into the GOM around southwestern Nova Scotia, weak (0.01–0.02 m s^{-1}) cyclonic circulation around Georges, Jordan and (part of) Wilkinson Basins and anticyclonic circulation of about the same magnitude around much of Georges Bank. However, the geostrophic constraint is broken in some locations such as in Northeast Channel where some of the southwestward flow through the Cape Sable region joins a 0.05 to 0.1 m s^{-1} outflow in the Channel, and in Great South Channel where part of the GOM transport turns southwestward and exits from the region. Over the modeled portion of the MAB, the smoother topography allows a broad, generally westward flow of about 0.02 m s^{-1} across the entire shelf. As indicated in Table 1, about 60% of the transport across the SS boundary flows around southwestern Nova Scotia into the GOM and about 20% enters the

TABLE 1. Predicted transports across the five sections indicated in Fig. 7 for various model runs. Positive values indicate flow into the GOM region and southwestward across the Jordan Basin section.

	Transports ($\times 10^5$ m^3 s^{-1})				
	SS boundary	SW Nova Scotia	Jordan Basin	Northeast Channel	Nantucket Shoals
Exponential setup (setdown) on SS (Fig. 2)	(−)7.0	(−)4.2	(−)1.1	(+)−2.8	(+)−1.4
Linear setup (setdown) on SS	(−)14.0	(−)7.5	(−)2.0	(+)−5.0	(+)−2.5
Alongshelf stress plus setdown on SS (Fig. 4)	−7.2	−5.9	−1.7	5.2	4.5
Alongshelf stress plus setdown on SS: nonlinear model	−7.1	−6.1	−1.7	5.7	4.7
Alongshelf stress plus setdown on SS: simple friction	−7.1	−6.0	−2.4	5.8	4.5
Alongshelf stress with cross-shelf variation, plus setdown on SS	−7.2	−6.1	−1.4	5.8	5.0
Cross-shelf stress (Fig. 5)	0.30	−0.14	−0.82	1.7	−0.30
Cross-shelf stress: nonlinear model	0.30	−0.20	−0.90	1.8	−0.36
Cross-shelf stress: simple friction	0.30	−0.24	−0.97	1.9	−0.55
Exponential setup on MAB (no radiation)	0.0	0.0	0.0	0.0	−0.22

MAB across Nantucket Shoals, while the transports along the Maine coast north of Jordan Basin and out through Northeast Channel are about 16% and 40%, respectively, of that across the SS boundary.

The dynamical considerations discussed in this subsection have important implications for the studies of Hayashi et al. (1986) and Isaji et al. (1982), which use a backward boundary condition consistent with the ISM. Hayashi et al.'s (1986) results confirm the significance of this boundary on an infinitely long shelf but would substantially overestimate the error associated with using a zero elevation condition on the SS boundary of the present model. While Isaji et al.'s (1982) solutions also illustrate the significance of the SS boundary, their prediction with zero alongshelf elevation gradient on this boundary, and hence a coastal setdown of over 0.4 m for each 0.1 Pa of stress, appears to overestimate the region's response to alongshelf wind stress forcing.

b. *Cross-shelf wind stress*

Theory (Csanady, 1980, 1981; Hayashi et al., 1986) generally suggests that, away from irregularities in the coastline, the response of coastal sea level to cross-shelf wind stress is substantially smaller than to alongshelf stress. This prediction is consistent with the observationally estimated coastal sea level gains presented by Noble and Butman (1979), Sandstrom (1980) and Thompson (1986).

In light of this and the theoretical prediction that any elevation change should decrease with distance offshore, we assume that the currents and elevations in the GOM associated with a 0.1 Pa cross-shelf wind stress on the backward (unmodelled) portion of the SS are substantially less than those in Fig. 2 and hence can be neglected (as a first approximation) compared with those due to local wind stress forcing. Therefore, we specify v_0 and ζ_0 to be zero on both the SS and MAB boundaries in the case of cross-shelf wind stress forcing.

4. Numerical model results for steady, uniform wind stress

a. *Spinup*

Before proceeding to describe the steady-state elevation and current patterns for alongshelf and cross-shelf wind stress forcing, we present a brief discussion of the spinup of the model from rest (zero elevation and velocity) to these steady states. The characteristics of the spinup are illustrated in Fig. 3, which shows the time-evolution of surface elevation at some coastal and offshore sites and of horizontal transports across some sections (see Fig. 7 for locations) for a 0.1 Pa alongshelf stress with a 0.1-m exponential setdown on the SS boundary, and for a 0.1-Pa cross-shelf stress. The spinup in both cases is characterized by an *e*-folding time scale of less than 20 hours such that, after about 50 hours, the elevations and transports are steady to within a few percent. This time scale is consistent with expectations based on the frictional spindown time scale of about 10 hours for the Bay of Fundy–Gulf of Maine system ($Q \approx 5$ for the dominant M_2 tidal frequency; Greenberg, 1979). This suggests that the results of the present study are most relevant to low-frequency wind stress variations with periods greater than 15 days ($3 \times 2\pi \times$ the spinup time).

The time-evolution of elevation and transport (Fig. 3) also includes higher-frequency variability that is consistent with expectations based on previous work. With cross-shelf forcing, an oscillation with period near 11 hours is apparent, similar to the lowest normal mode oscillation found by Beardsley and Haidvogel (1981) although the oscillation in the present model is damped much more rapidly by the increased (and more realistic) friction. [Note, however, that both Beardsley and Haidvogel's (1981) and the present model probably underestimate the approximately 13-h period (Garrett, 1974) of this mode because of the clamped boundary across the Bay of Fundy.] With alongshelf forcing and an elevation setdown on the SS boundary, this oscil-

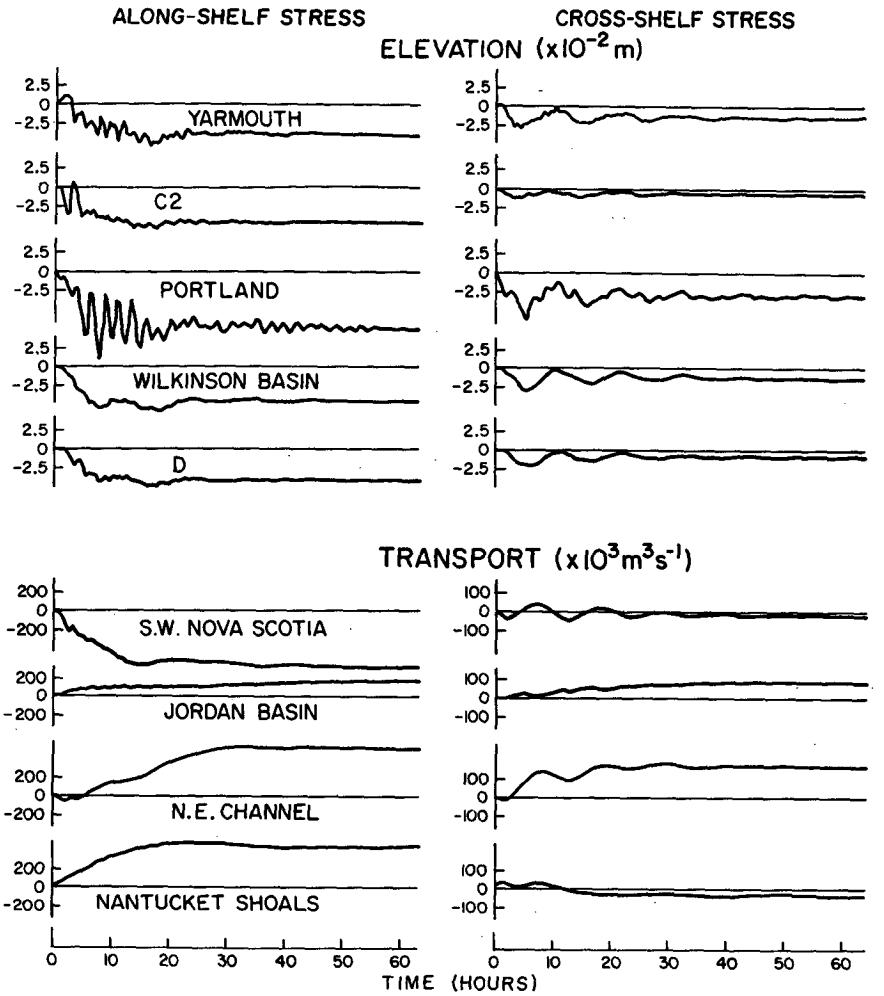

FIG. 3. The time-evolution during model spinup of surface elevation at several sites in the model domain (Fig. 1) and of transport across the sections indicated in Fig. 7 for a 0.1 Pa alongshelf wind stress with a 0.1 m exponential setdown across the backward boundary, and for a 0.1 Pa cross-shelf stress.

lation is less apparent; instead, the variability in coastal elevation is dominated by fluctuations with periods of a few hours, similar to those reported by Beardsley and Haidvogel (1981) for the MAB. These fluctuations (which are also present during spinup to the SS setdown alone) appear to be associated with coastal-trapped waves that are generated by the setdown on the SS boundary and which propagate along the coastline arriving increasingly later at positions to the southwest.

b. Alongshelf wind stress

The steady-state model results (after 96 hours) for elevation and current, and the transports across the selected sections, for forcing by a spatially uniform alongshelf wind stress of 0.1 Pa with a 0.1 m exponential setdown on the SS boundary are shown in Fig. 4 and Table 1 respectively. On the SS east of the Cape Sable region, the dominant influence is from the setdown specified on the backward boundary (its contribution is simply the negative of that in Fig. 2). However, with increasing distance in the forward direction, the contribution from wind stress forcing over the model domain generally becomes increasingly important and clearly dominates in the MAB. Thus, in the case of alongshelf stress, it appears that forcing over the backward (unmodeled) portion of the SS has a significant, but not dominant, influence on the GOM region.

The predicted elevation and current patterns (Fig. 4) in the GOM show qualitative similarity to some of the patterns in Csanady's (1974) idealized model, and Beardsley and Haidvogel's (1981) and Isaji et al.'s (1982) numerical models, but there are also significant differences. Consistent with theoretical expectations, there is generally flow in the direction of the wind stress along the SS, GOM and MAB coasts and over the relatively shallow, offshore Banks (Browns and Georges), a counterflow between Georges Bank and the coastal flow in the GOM, and cross-shelf elevation variations

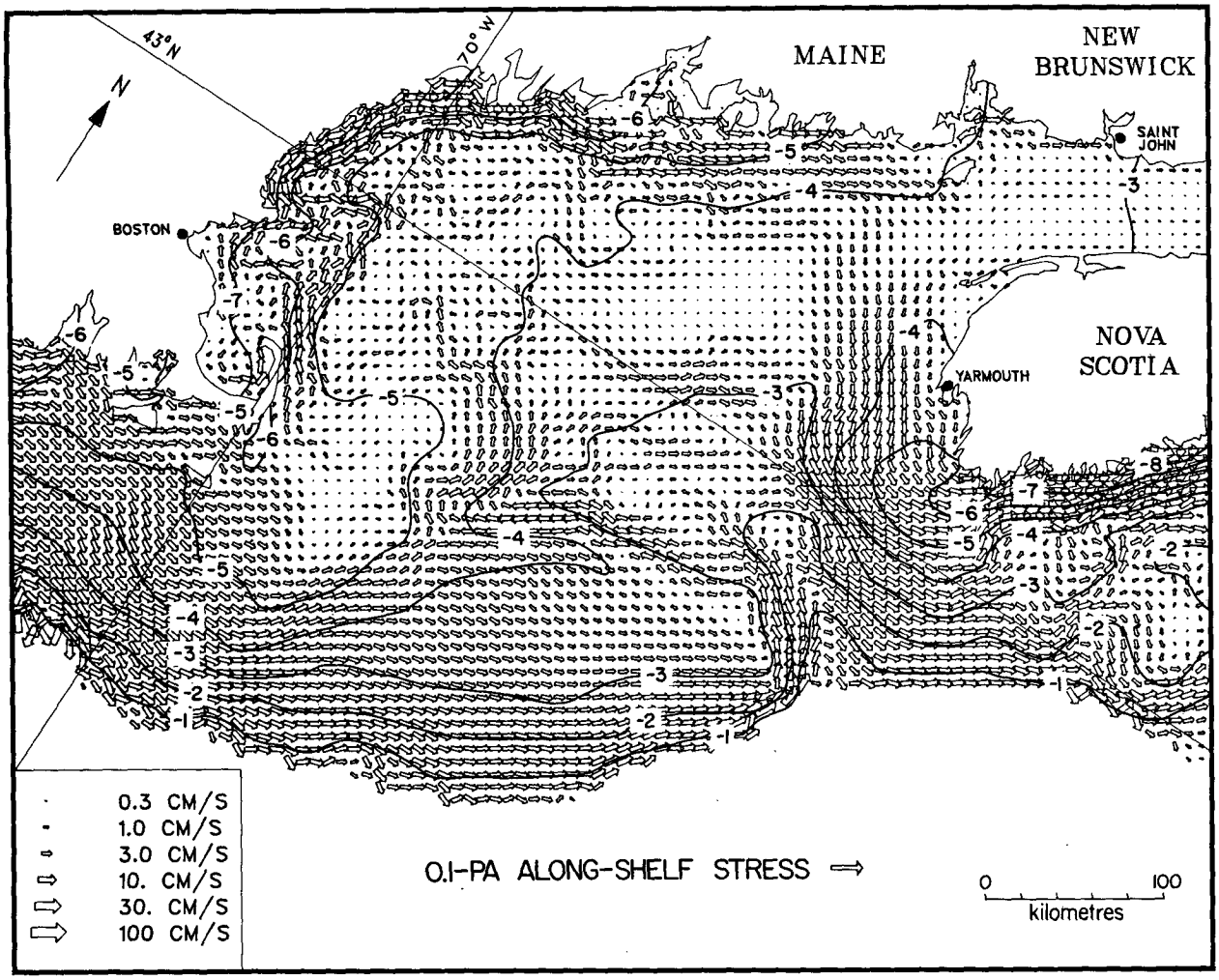

FIG. 4. Predicted elevations (cm) and currents for a 0.1 Pa alongshelf wind stress with a 0.1-m exponential set-down across the backward boundary.

consistent with an approximate geostrophic balance for these flows. Except on the SS where the backward boundary condition's influence dominates, the coastal flows and the associated setdown generally increase with distance in the forward direction in areas where the coastline is roughly parallel to the stress (as expected from the ATWM). In contrast, the flow and elevation contours are primarily orthogonal to the wind stress along the western GOM coast, off Yarmouth and in Northeast Channel, presumably due to the indentation of the coastline and the Channel's topography. Thus, as found by previous investigators, a northeasterly (i.e., in the opposite direction to that in Fig. 4) wind stress contributes to anticyclonic circulation over Georges Bank and cyclonic circulation over the inner GOM (with a transport of 1.7×10^5 m^3 s^{-1} across the Jordan Basin section for each 0.1 Pa of stress). Also as expected, the radiation condition on the forward boundary allows a substantial sea level setdown and a transport into the MAB of the same order as that into the GOM (Table 1).

On the other hand, the present predictions have considerably more detail than those of Csanady (1974) and Isaji et al. (1982), and there are qualitative differences from Beardsley and Haidvogel's (1981) predictions for the eastern GOM (presumably due to the specification of zero elevation on their SS boundary in the Cape Sable region) and from Isaji et al.'s, 1982, predictions for the SS and offshore regions (probably due to their SS boundary condition and their use of a false bottom beyond the shelfbreak). A striking feature of the present results is that the cross-shelf transport through Northeast Channel is in the opposite direction to the surface Ekman transport (see section 7 for further discussion) and of the same order of magnitude as the alongshelf transport (Table 1). Although some of this inflow (for southwesterly wind stress) turns eastward onto the SS, most of it moves westward into Georges Basin forming the alongshelf counterflow and then meanders northwestward through Wilkinson Basin to supply the anticyclonic coastal flow in the western GOM. The circulation in the inner GOM is somewhat

irregular, with suggestions of substantial topographic control over such features as Jeffreys Bank and the ridge between Jordan and Crowell Basins.

c. *Cross-shelf wind stress*

The predicted elevations, currents and transports for a spatially uniform cross-shelf (offshore) wind stress of 0.1 Pa, shown in Fig. 5 and Table 1, are generally much smaller than those due to the alongshelf stress, as expected, and form patterns that are qualitatively consistent with expectations for a partially enclosed basin. Along the western GOM coast and off Yarmouth where the stress is roughly parallel to the local coastline, there is depth-averaged flow in the direction of the wind stress, while over the broad central portion of the GOM there is a rather diffuse geostrophically balanced counterflow. On average, there is a setdown of about 0.01 m over the GOM, but there are a local relative setup along the western GOM coast and a similar setdown off Yarmouth providing an approximate geostrophic balance for the coastal flows. There is also increased setdown in a nearshore band about 20–30 km in width along the entire northwestern GOM, balancing the offshore wind stress.

In areas with smooth topography in the outer portion of the modeled region, the (depth-averaged) currents are generally in a southward to southwestward direction, qualitatively consistent with Ekman transport including reduced Ekman veering with decreased depth (e.g., on Georges Bank). On the SS, there is also southwestward flow near the coast while in the MAB there is a northeastward coastal flow, both of which are probably driven by the small component of the wind stress that is parallel to the local coastline. The somewhat irregular current pattern over much of the SS becomes more uniform in the Cape Sable region but, as for alongshelf stress forcing, it is substantially perturbed by Northeast Channel. In fact, the largest transports across the selected sections for this case of offshore stress (Table 1) are an inflow through the Channel (in the opposite direction to the stress) and an anticyclonic

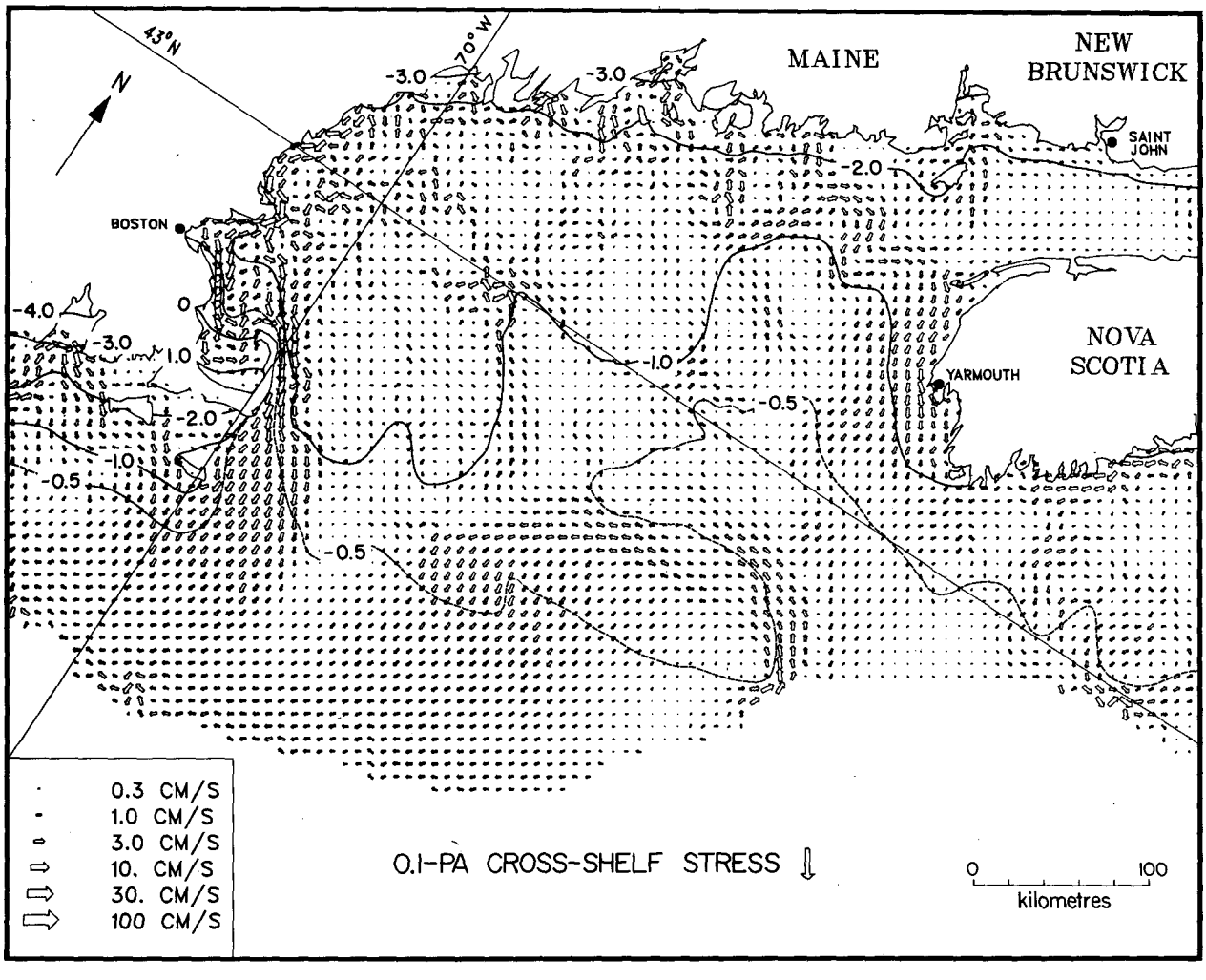

FIG. 5. Predicted elevations (cm) and currents for a 0.1 Pa cross-shelf (toward 146°T) wind stress.

circulation around Jordan Basin. The former is joined by a small flow across the Channel from the SS and generally proceeds westward, in part along the northern side of Georges Bank, to supply the various branches of the northwestward counterflow across the GOM.

5. Model sensitivity

a. Backward boundary condition

The SS boundary condition has already been discussed in sections 3 and 4b. Under the present assumption of linearity, the influence of increasing/decreasing the magnitude of the elevations and currents on this boundary, while maintaining an exponential cross-shelf decay, is clear: the elevation changes and currents in the model domain that are associated with the boundary forcing (Fig. 2) increase/decrease proportionately in strength, hence the forward extent of the boundary's influence is increased/decreased and the total elevation and current patterns may be altered.

In addition, the elevations and currents in the model are dependent on the cross-shelf structure of ζ_0 and v_0 on the SS boundary. This structure is unlikely to be accurately reproduced by the ATWM as illustrated in Fig. 2 where the coastal current spreads rapidly across the shelf due to topographic irregularities. Thus, it is possible (and, as discussed in section 6, probable) that a uniform current distribution across the backward boundary (consistent with the ATWM predictions for a step-shelf) is more appropriate. The sensitivity of our results to such a difference in the backward boundary condition is illustrated in Fig. 6 which shows the elevation and current *differences* between the case of a 0.1 m specified coastal setup with a *linear* decrease offshore on the SS boundary and the previous case (Fig. 2) of the same coastal setup but with an *exponential* decrease away from coast (both with zero wind stress).

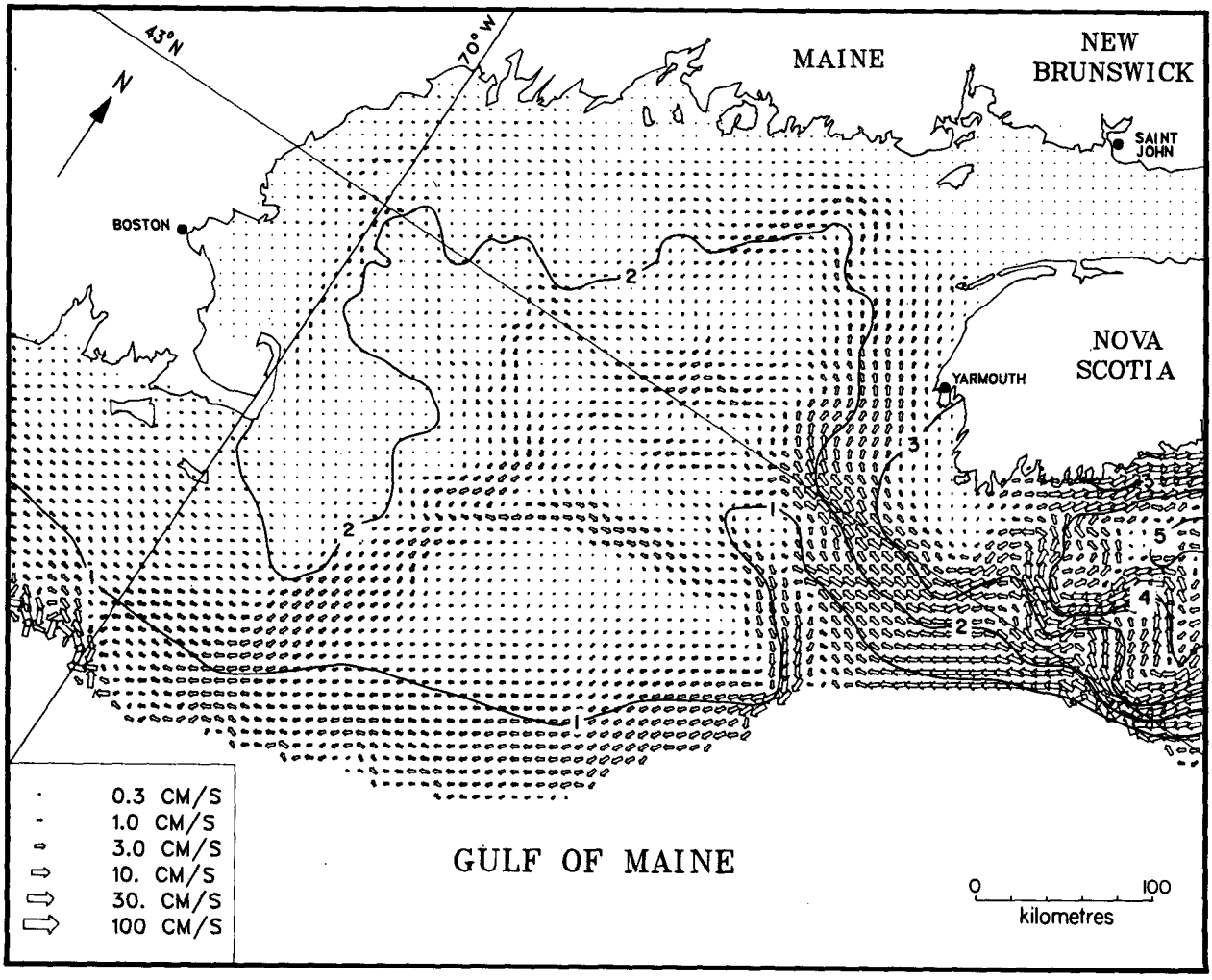

FIG. 6. The differences in elevation (cm) and current between the case of a setup across the backward boundary which varies linearly from 0.1 m at the inshore edge to 0.0 m at the offshore edge, and the case of a setup which varies exponentially on a scale of 39 km away from its coastal value of 0.1 m.

As can be seen from the sectional transports in Table 1, the primary domain-wide influence of the different cross-shelf structure on the backward boundary, with the coastal elevation unchanged, is an approximate doubling of the strength of the circulation, consistent with the ATWM prediction (Csanady, 1978) that the effective strength of the boundary forcing is proportional to $\int \zeta(x)dx$. The other significant difference is that, with the linear elevation decrease offshore, there is reduced southwestward flow near the Nova Scotian coast (and hence a northeastward flow in the difference plot, Fig. 6), but the influence of this difference is largely confined to the SS. Thus, both the coastal value and cross-shelf structure of the elevation on the SS boundary of the present model have a significant quantitative influence on the circulation in the GOM region associated with alongshelf wind stress. Evidently, if a linear variation in ζ across the Scotian Shelf is assumed, the coastal elevation must be roughly halved to maintain the same transports as with the exponential variation used in Fig. 2.

b. *Forward boundary condition*

Based on the theoretical guidance provided by the ATWM, the conditions specified on the forward cross-shelf boundary are not expected to have a significant influence on the elevations and currents away from this boundary. Furthermore, it is evident from the numerical solutions shown in Figs. 2 and 4–6 that, even with values of zero specified for ζ_0 and v_0 on the MAB boundary, the radiation condition allows elevations and currents in the MAB boundary region that are qualitatively consistent with those expected on the basis of the ATWM.

To verify the insensitivity of the present results to the MAB boundary condition, an additional run was made with a *fixed* 0.1 m coastal setup and exponential decay in elevation across the MAB boundary as the only forcing (note that, in the absence of wind stress, it was necessary to eliminate the adjustment permitted by the radiation condition in order to maintain a significant setup along this boundary). Predicted elevations and currents (not reproduced here) and transports (Table 1) were confined within a few grid squares of the boundary, in stark contrast to the analogous case (Fig. 2) of setup on the SS boundary. This result clearly demonstrates that the forward direction is the preferred direction of influence and that the model predictions are not sensitive to the MAB boundary condition.

c. *Nonlinearity*

To examine the significance of the nonlinearities associated with the advective terms and the quadratic bottom stress law in the fully nonlinear barotropic equations of motion and continuity in the presence of strong tidal currents, we have obtained numerical solutions (following Greenberg, 1983) to these equations using the quadratic stress law (4) and with (i) a 0.1 Pa alongshelf (southwesterly) wind stress, a 0.1 m exponential setdown (in the radiation condition) on the SS boundary and M_2 tidal elevations specified (following Greenberg, 1983) on all open boundaries; (ii) a 0.1 Pa cross-shelf wind stress with only tidal elevations specified on the open boundaries; and (iii) no wind stress, but with tidal elevations specified on the open boundaries. Then, subtraction of the tidally driven [i.e., (iii)] residual elevations, currents and transports from the tidally-driven plus wind-driven [i.e., (i) and (ii)] values yields the fully nonlinear model's predictions for alongshelf and cross-shelf stress. Comparison of the predicted elevations and currents (not shown), and transports (Table 1) with those from the linear model indicates that the linear model reproduces the qualitative features, and in most places the strength to within about 10%, of the nonlinear model's response (the discrepancies in current are largely confined to the vicinity of the open boundaries, the SS, Northeast Channel, Georges Basin and the western GOM, and may be partially due to influences of the irregular shelfbreak boundary and the lack of steadiness of the present solutions in local areas of relatively weak friction). This suggests that the present linearization of the quadratic stress law is an adequate approximation (at least for wind stress magnitudes of order 0.1 Pa) and the asymmetric coastal sea level response to wind stress reported by Noble and Butman (1979) is not part of a barotropic model's steady response to tidal and spatially uniform wind stress forcing.

d. *Parameterization of bottom stress*

In addition to checking the adequacy of (3a, b) as a linearization of the quadratic stress law in the presence of strong tidal currents, it is instructive to examine the sensitivity of the present solutions to the general representation of bottom friction. To do this, we have repeated the linear model runs for 0.1-Pa wind stresses in the alongshelf and cross-shelf directions with the simple linear bottom stress law

$$(\tau_x^b, \tau_y^b) = \rho c_D \bar{Q}(u, v), \tag{12}$$

where $\bar{Q}$ is a mean current speed taken to have a spatially uniform value of 0.50 m s^{-1}. In the alongshelf stress case, the same values of ζ_0 and v_0 are specified on the SS boundary as before, although the idealized ATWM solutions (section 3) suggest that the representation of friction on the unmodeled backward portion of the SS may influence these values and hence the elevations and currents in the model domain.

The results of these runs (elevations and currents are not reproduced here, but see the transports in Table 1) indicate that the qualitative features of the GOM region's response to both alongshelf and cross-shelf wind stress forcing are not strongly dependent on the parameterization of bottom stress, provided that the influence of the background tidal currents is at least crudely included. However, there are quantitative

changes ($\approx$0.005 m for ζ and $\approx$0.05 m s^{-1} for u, v) in some parts of the region associated with the different parameterizations. In particular, in areas with strong tidal currents such as Nantucket Shoals, central Georges Bank and off southwestern Nova Scotia, the 0.50 m s^{-1} value used for $\bar{Q}$ in (12) underestimates the background currents, and hence the wind-driven currents are stronger with less veering away from the direction of Ekman transport. In contrast, there are reduced wind-driven currents and coastal sea level setdowns in areas with weak tidal currents such as along the western and northwestern coasts of the GOM and on the nearshore portion of the SS, presumably because the above value of $\bar{Q}$ overestimates the background current speed in these areas.

e. *Cross-shelf variation in alongshelf stress*

The results presented thus far are for spatially uniform wind stress forcing, but it is appropriate to estimate the significance of spatial variability in the stress. For example, Saunders' (1977) summary of wind stress observations over the region suggests that the seasonal mean stress magnitudes are significantly larger offshore than near the coast. To provide an estimate of the significance of such a variation, and of a nonzero curl in the wind stress, Table 1 also includes the steady state transports for the case of forcing by an alongshelf (southwesterly) stress which is uniform in the alongshelf direction but which varies linearly in the cross-shelf direction ranging from a value of 0.067 Pa at the minimum x position to 0.13 Pa at the maximum x position. This stress field has an x-averaged value similar to the 0.1-Pa value in the earlier spatially-uniform cases, and a 0.1-m coastal setdown with an exponential decay offshore is specified on the SS boundary as before. The elevations, currents and transports show the same qualitative features as for spatially uniform alongshelf stress, but there are quantitative differences. There are reduced northeastward currents and coastal setdowns along the western and northwestern GOM coasts, associated with the reduced stress over the inner GOM, and reduced inflow along Cape Cod and in Georges Basin supplying this coastal flow. On the other hand, associated with the increased stress offshore, there are stronger northeastward currents over the outer portions of the MAB, Georges Bank and the SS, and increased inflow through Northeast Channel. These elevation and transport differences are generally less than 15% which suggests that the region's response to alongshelf wind stress is not strongly dependent on the forcing's spatial structure. However, these results also indicate that if the stress field is to be approximated as spatially uniform, the average value over the area should be used rather than say a local coastal value.

6. Comparison with observations

a. *Coastal sea level gains*

The model predictions of the coastal sea level changes at various GOM sites for a 0.1 Pa alongshelf wind stress with five different backward boundary conditions [$\zeta = 0$ for all x, and 0.1 and 0.05 m coastal sea level setdowns with both exponential and linear decreases offshore (before radiative adjustment)] are presented in Table 2 together with Noble and Butman's (1979) and Thompson's (private communication, 1985; henceforth T2) observed changes. The boundary condition $\zeta_0 = 0$ clearly underestimates sea level variations, particularly near the SS boundary, and there is some suggestion that the case $\zeta_0 = 0.05$ m exponential

TABLE 2. Coastal sea level changes for a 0.1 Pa alongshelf wind stress, as predicted by the present model with five different backward boundary conditions and as observed.

	Model Predictions ($\times 10^{-2}$ m)					Observations ($\times 10^{-2}$ m)	
Location	$\zeta_0 = 0$	0.1-m Exp	0.1-m Lin	0.05-m Exp*	0.05-m Lin*	Noble and Butman**	Thompson***
Halifax	—	—	—	—	—	−11.5	−3.3
Yarmouth	−0.6	−4.1	−6.7	−2.3	−3.6	−8.3	−4.9
Eastport	−1.4	−4.4	−6.7	−2.9	−4.0	−6.8	—
Bar Harbor	−2.3	−5.2	−7.5	−3.8	−4.9	—	−3.4
Rockland	−3.3	−6.2	−8.4	−4.8	−5.6	−12.0	—
Portland	−5.0	−7.8	−10.0	−6.4	−7.5	−12.0	−5.8
Portsmouth	−4.7	−7.5	−9.7	−6.1	−7.2	—	−6.0
Boston	−5.2	−8.0	−10.1	−6.6	−7.6	−11.5	−6.0
Cape Cod	−4.7	−7.5	−9.6	−6.1	−7.1	—	−5.6
Nantucket	−3.4	−5.7	−7.4	−4.5	−5.4	−9.9	−5.4

* The values for these cases are estimated from those in the first three columns under the assumption of linearity.

** The values listed for Noble and Butman (1979) are obtained by dividing the values in the third column of their Table 3 by $\rho_{air} = 1.2$ kg m^{-3} and $C_{10} = 1.6 \times 10^{-3}$.

*** These values, calculated using spatially averaged wind stress for the GOM and SS region (K. R. Thompson, private communication, 1985), are revised from those in Thompson (1985).

also leads to underestimates. For all of the other boundary conditions, the predicted changes have similar spatial structure to that observed and the magnitudes lie within the range of the observational estimates. This confirms that the qualitative features of the region's sea level response to low-frequency, alongshelf wind stress forcing can be reproduced by the present model. However, determination of the most appropriate backward boundary condition requires further consideration of the discrepancy between Noble and Butman's (1979) and Thompson's (T2) observed gains, and of the uncertainties in the model predictions and observations.

There are two factors that may contribute to Noble and Butman's (1979) sea level gains being higher than those predicted by the present model which, as discussed earlier, is most appropriate to wind stress variations with periods of 15 days and longer. Noble and Butman's (1979) gains are for the period range of 2.5–25 days, while Noble et al. (1985) have shown that most of the wind energy in this band is at periods substantially less than 15 days, and that, at least in part of the region (Georges Bank), the current gains decrease at longer periods with a resonance-like response at periods near 8 days. Thus, comparison of their results with steady-state model results may be inappropriate. Second, Noble and Butman (1979), as well as Sandstrom (1980), used coastal wind observations while numerous authors (e.g. Saunders, 1977; Noble et al., 1983; Smith, 1985) have found a significant offshore increase in wind stress on the SS and in the GOM and MAB. Considering this and the results of the last section, it seems likely that Noble and Butman's (1979) and Sandstrom's (1980) sea level gains are substantial overestimates of the actual gains per unit stress averaged over the region.

On the other hand, Thompson (T2) has used monthly maps of atmospheric surface pressure to derive surface wind stress, and linear multiple regression to obtain the coastal sea level response (at periods exceeding two months) to the spatially averaged stress over the GOM and SS. Although there is some uncertainty in the appropriate reduction and rotation between geostrophic and surface wind velocity, Thompson's (T2) observed gains should be most appropriate for comparison with the steady response of the present model to steady, spatially uniform stress. Comparison of the predicted and observed gains in Table 1 suggests that a 0.1 m coastal setdown with a linear decrease offshore overestimates the influence of alongshelf stress over the unmodelled portion of the SS, but the predicted gains for the other three specified setdowns generally lie within ±40% of Thompson's (T2) observational estimates. The most appropriate of these cases is unclear from this comparison but current observations off southwestern Nova Scotia (next subsection) suggest that the 0.05 m linear case is the best approximation.

The model predictions of the coastal sea level changes associated with both alongshelf and cross-shelf stress, as well as the uncertainty in these predictions, are summarized in Fig. 7 which shows the direction of the stress that results in the maximum setup at various locations, and the magnitude of the setup associated with a 0.1 Pa stress in this direction (maximum setdowns of the same magnitude are associated with stresses in the opposite direction). The uncertainty in the predictions is derived from the sensitivity analysis of section 5, with the major uncertainty (within the context of the present barotropic model), arising from the specification of the backward boundary condition. Predictions are presented for five different conditions on this boundary: $\zeta_0 = 0$ for all x, $\zeta_0 = (0.1, 0)$ plus exponential decrease offshore, $\zeta_0 = (0.1, 0)$ plus linear decrease, $\zeta_0 = (0.046, 0.019)$ plus exponential decrease, and $\zeta_0 = (0.046, 0.019)$ plus linear decrease, where the two parenthesized numbers refer to the coastal elevations (in m) for 0.1 Pa stresses in the $-y$ and $-x$ directions, respectively, and where v_0 is obtained from geostrophy. For comparison, Thompson's (T2) observational results are also shown in Fig. 7. The observational error bounds represent the 95% confidence limits on the sea level changes.

In general, the model predicts maximum setups (setdowns) for wind stresses in a roughly southwestward (northeastward) direction. The predicted magnitudes vary with location in the general manner expected from the ATWM, with the largest values occurring in the northwestern GOM where the coastline in the backward direction is largely alongshelf (in the present terminology). Considering the observational uncertainties, the model predictions with $\zeta_0 = (0.1, 0)$ plus exponential decrease and $\zeta_0 = (0.046, 0.019)$ plus linear decrease as backward boundary conditions show reasonable overall agreement with the observations, although there appears to be a small discrepancy in direction, particularly in the western GOM.

b. *Current gains off southwestern Nova Scotia*

Figure 8 shows a comparison between the predicted currents for a 0.1 Pa alongshelf wind stress and wintertime middepth current gains derived from measurements off southwestern Nova Scotia (Smith, 1983, 1986). Model results are shown for three backward boundary conditions; $\zeta_0 = 0.0$ m; $\zeta_0 = 0.1$ m, exponential; and $\zeta_0 = 0.05$ m, linear. Here the additional estimates of model uncertainty (shown only for the 0.1 m, exponential case, but of similar magnitude for the other two cases) are based on the spatial variability in the currents at the four grid points surrounding the mooring site. Thus the large error bars on the prediction at C4 reflect an exceptionally high shear in the model flow field associated with veering of the current in Northeast Channel (Fig. 4).

The observed current gains are calculated from a frequency-dependent linear multiple regression analysis

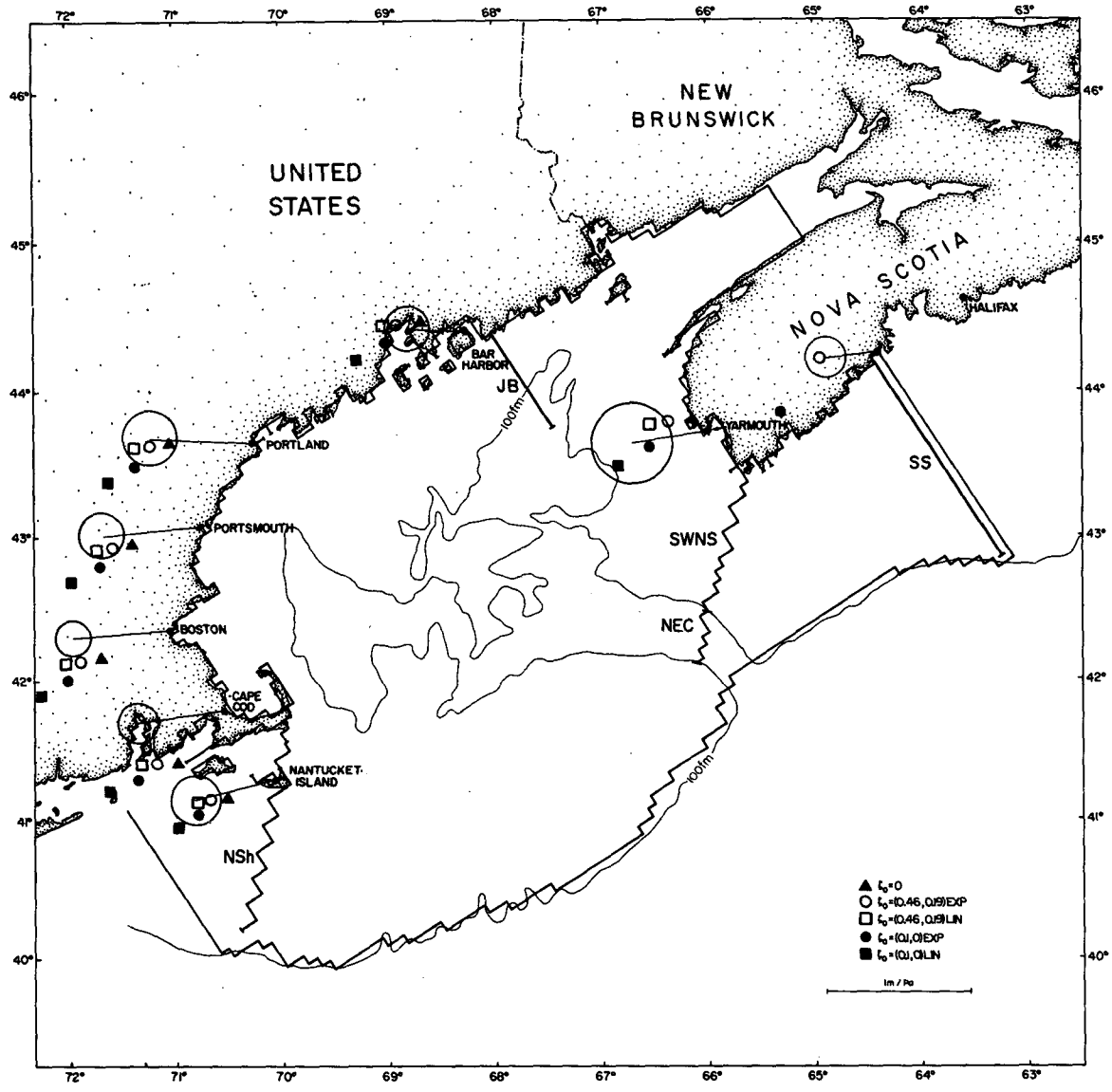

FIG. 7. Model predictions with five different backward boundary conditions [(▲) $\zeta_0 = (0, 0)$; (○) $\zeta_0 = (0.046, 0.019)$, exponential; (□) $\zeta_0 = (0.046, 0.019)$, linear; (●) $\zeta_0 = (0.1, 0)$, exponential; (■) $\zeta_0 = (0.1, 0)$, linear] and Thompson's (private communication, 1985) observational estimates (with 95% confidence intervals) of the coastal sea level changes associated with a spatially uniform wind stress. The changes are maximum for wind stress in the direction indicated and zero for stress in the orthogonal direction. The local magnitude of the maximum gain is indicated by the length of each stick. Also indicated are the sections referred to in Fig. 3 and Table 1 (SS: Scotian Shelf; JB: Jordan Basin; SWNS: Southwestern Nova Scotia; NEC: Northeast Channel; NSh: Nantucket Shoals).

using current meter data and stresses derived from wind measurements (Smith, 1986) at Sable Island, an offshore site on the SS. The current meter data were taken from the winter season (October 1979 to March 1980) when the stratification of the coastal waters is least.

Mid-depth current measurements have been used for comparison with the barotropic model predictions, based on the results of a simple diagnostic Ekman model (e.g., Csanady, 1976; Smith, 1983) which indicates that when the Ekman-layer thickness is less than half of the total depth, the mid-depth current forced by alongshelf wind stress is in geostrophic balance with the pressure gradient induced by the cross-shelf sea surface slope and is nearly equal to the depth-averaged current. The current gains that are compared with the steady model response are taken from the zero frequency band, i.e., they are related to the covariance between the wind stress and current. However, the response coefficients in the spectral bands centered on 8- and 4-day periods are of similar magnitude and are statistically indistinguishable from those at zero frequency, and their phase is nearly invariant (within

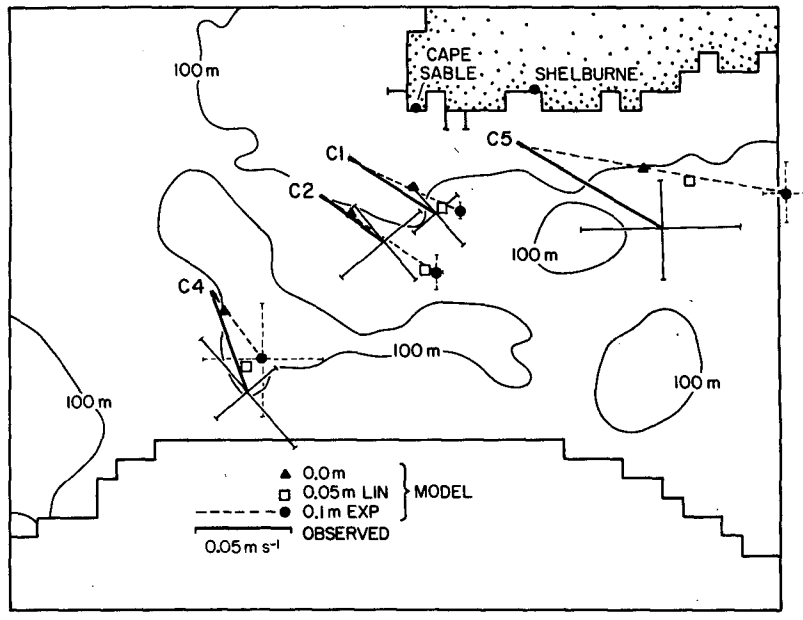

FIG. 8. Predicted current gains [(▲) no setup on SS; (●) 0.1 m, exponential; (□) 0.05 m, linear] and observed wintertime mid-depth current gains (Smith, 1986) off Southwestern Nova Scotia for a 0.1 Pa alongshelf wind stress. The error bars on the observed responses are based on the 95% confidence limits for the transfer coefficients between the observed wind stress and current components.

±20°) over this portion of the frequency spectrum (Smith, 1986). This behavior is consistent with the model estimate of less than 1 day for the spin-up time of the entire GOM region. The substantial agreement between the predicted and observed currents supports the choices of mid-depth currents as representative of the depth-averaged currents and of Sable Island winds as representative of forcing over the SS. It also indicates that two of the three backward boundary conditions used in the model sensitivity runs are reasonable approximations. Perhaps the best agreement is found for the 0.05 m linear case, particularly at C5 which is closest to the SS boundary, but apart from at that site, the results for the 0.1 m exponential case compare as well considering the level of uncertainty.

The linear regression analysis also reveals that at low frequencies, the current gain at each mooring site is largest when the wind stress acts in roughly the alongshelf direction and the current direction is consistent with that predicted by the barotropic model, i.e., parallel to local isobaths (Fig. 8). The largest response occurs at the C5 site off Shelburne where the friction is weakest and the coastal barrier results in a divergence in the offshore Ekman flux at the surface. On the other hand, the response off Cape Sable is weaker because of enhanced friction (stronger tidal currents) and the removal of the coastal barrier.

The measured response to cross-shelf wind stress is generally strongest near the surface and weaker or insignificant at greater depths (Smith, 1986). However, the high levels of statistical uncertainty in the associated current gains and the lack of an adequate indicator of the depth-averaged current preclude comparison with the barotropic model predictions.

7. Regional dynamics

The local dynamical balances at selected sites within the model are displayed for alongshelf and cross-shelf wind stress forcing in Figs. 9 and 10, respectively. The results for alongshelf stress are those for a 0.1 m, exponential setdown on the backward boundary.

With an alongshelf stress, the momentum balances where the current follows isobaths in the downwind direction are consistent with the ATWM (also see Fig. 4). For example, at sites A on Georges Bank and C5 on the SS, the cross-shelf balance is geostrophic while bottom friction balances wind stress in the downstream direction. At sites C1 on the SS and NSFE1 in the MAB, the flow deviates slightly from the wind direction to follow local isobaths but the cross-*stream* momentum balance is still nearly geostrophic and a larger bottom friction (particularly at C1) balances the downstream components of wind stress and pressure gradient.

At the deep-water site NEC3 in Northeast Channel, however, the wind stress and bottom friction are negligible, and the cross-channel pressure gradient balances a geostrophic flow that turns onshore (Fig. 4) to follow isobaths, presumably because of vorticity constraints.

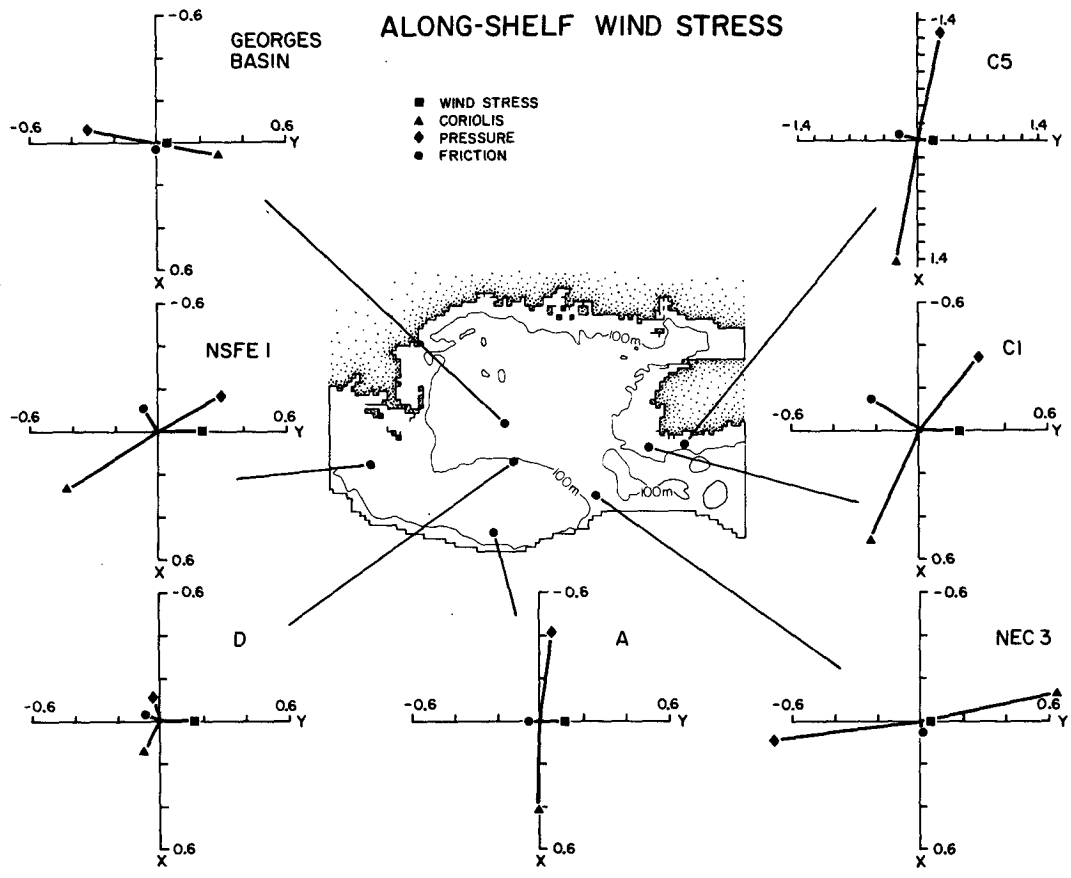

FIG. 9. Momentum balances (in units of 10^{-5} m s^{-2}) at selected sites within the model domain for a 0.1 Pa alongshelf wind stress with a 0.1 m exponential setdown across the SS.

This current continues to turn to the west until, in the region between the Georges Basin site and site D, it opposes the driving wind stress. In this region, as at the Georges Basin site, the wind stress is balanced by a component of the pressure gradient with the cross-stream balance remaining geostrophic. At site D the balance is even more complex. The downstream component of wind stress is opposed by the pressure gradient and bottom friction while the cross-stream balance is significantly ageostrophic. Clearly, these balances, caused by large-scale adjustments of the pressure field and vorticity constraints imposed by the complex topography, are inconsistent with the idealized ATWM.

The dominant response to cross-shelf wind stress at sites A and D on Georges Bank (Fig. 10) is not unlike that in a simple surface Ekman layer; the wind stress is balanced primarily by the Coriolis force on the depth-averaged current, which is roughly 90° to the right of the wind stress. The weak bottom friction, which opposes the current, is reinforced by an along-bank pressure gradient at both of these sites. The pressure gradient becomes more prominent at the SS and MAB sites (C1, C5, and NSFE1) where it opposes the wind stress permitting the current to turn offshore. In Northeast Channel (NEC3), the strong cross-channel component of the pressure gradient geostrophically balances the flow into the GOM while the along-channel component of pressure gradient counteracts the wind stress and weak bottom friction. A similar balance obtains at the Georges Basin site.

It is noteworthy that the model predictions for Georges Bank do not agree with Brink's (1983) idealized model predictions which, treating the Bank as infinitely long and neglecting coastal barriers, indicate that cross-bank wind stress should be more effective than along-bank stress in driving currents. The present model predicts (cross-shelf, alongshelf) currents of (0.004, −0.011) m s^{-1} and (0.001, 0.045) m s^{-1} at site A for 0.1 Pa cross-shelf and alongshelf stresses respectively, and currents of (0.004, −0.018) m s^{-1} and (0.009, 0.035) m s^{-1} at site D for the same stresses. The predictions for site A are in qualitative agreement, however, with the observed current gains reported by Noble et al. (1983) and Noble et al. (1985) although their results are mainly for periods of less than 15 days.

Finally, the dynamical balances and predicted

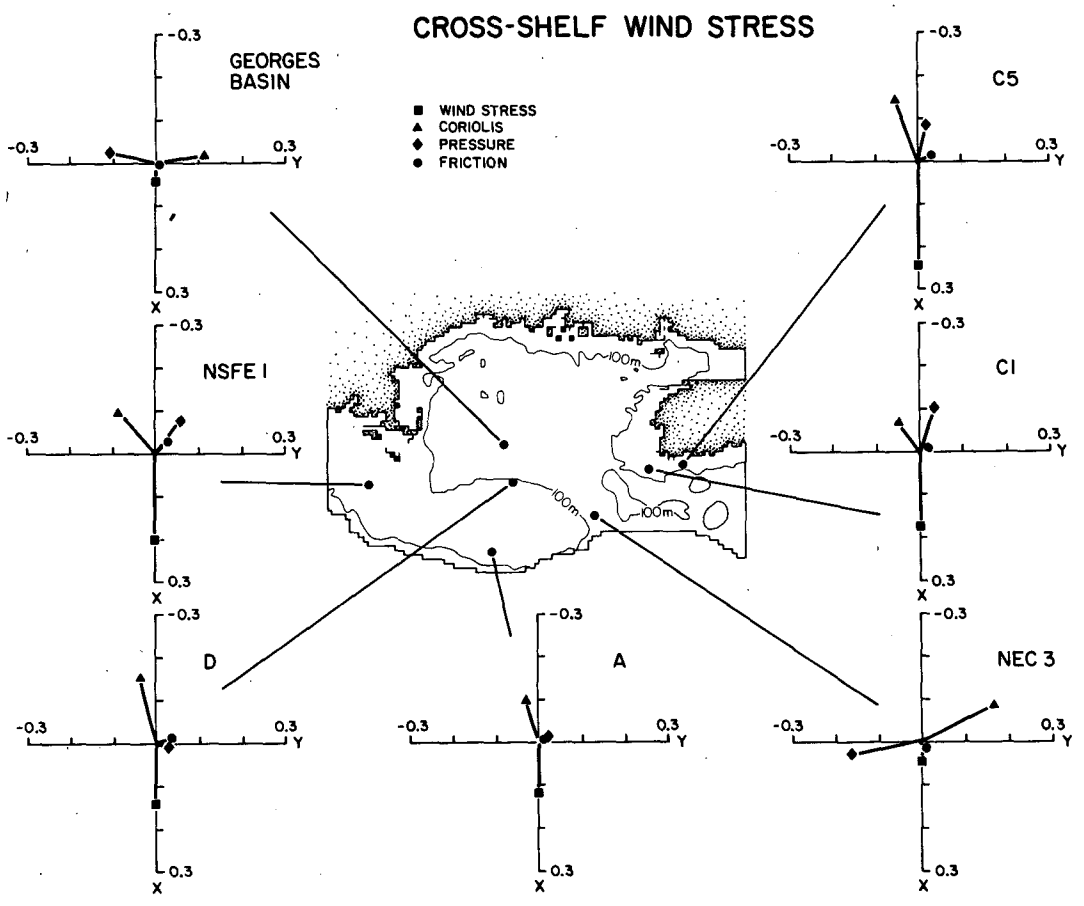

FIG. 10. Momentum balances (in units of 10^{-5} m s^{-2}) at selected sites within the model domain for a 0.1 Pa cross-shelf wind stress.

transports in Northeast Channel are in qualitative agreeement with the observational results of Ramp et al. (1986) which show that, in winter, transport through the Channel is associated with sea level changes in the GOM and both alongshelf and cross-shelf wind stress in the same sense as predicted here.

8. Discussion and conclusions

The present numerical model results suggest that the steady-state response of the GOM and adjacent regions to steady wind stress has many of the dynamical properties of the idealized ATWM (Csanady, 1978) but with substantial influences from the indentation of the coastline and the irregular bottom topography. The component of the stress that is parallel to the large-scale coastline (running approximately along 56°T) is generally much more effective than the cross-shelf component in driving currents and elevation changes, and away from coastline indentations and pronounced topographic features, the circulation is primarily in this alongshelf direction. The wind stress over a particular area generally has a significant influence on the circulation and elevation field a considerable distance in the forward direction so that, for example, the response of the GOM to alongshelf stress includes a significant contribution from forcing over the entire SS. Thus, one of the primary uncertainties in the present model, which only includes about one-half of the SS, is the appropriate condition for the SS boundary. Our results together with coastal sea level observations from Halifax (Noble and Butman, 1979; Sandstrom, 1980; Thompson, 1986, T2) suggest that the models of Isaji et al. (1982) and Hayashi et al. (1986), which use SS boundary conditions appropriate to an infinite shelf, overestimate the influence of forcing over the SS on the GOM's response to alongshelf stress. On the other hand, a significant component of the GOM's response to this stress appears to be neglected in Beardsley and Haidvogel's (1981) and Greenberg's (1983) models because of their specification of zero elevation on the SS boundary. With the present observational uncertainties, it is not possible to determine conclusively the appropriate SS boundary condition. However, our results do suggest that a 0.05-m coastal setup for each

0.1 Pa of alongshelf stress, with a linear decrease offshore, is a reasonable approximation.

The model, which includes the influence of the relatively strong background tidal currents on the bottom stress, has a spinup time from rest of 20 hours, suggesting that its results should be most relevant to wind stress variations with periods of about 15 days and longer. This spinup time scale is much shorter than that for the GOM in the Beardsley and Haidvogel (1981) model which appears to overestimate the spinup time because of the neglect of tidal current influences on the bottom friction and the use of clamped cross-shelf boundary conditions (not allowing the outward propagation of gravity waves).

The maximum sea level setdown/setup at various coastal sites in the model is found to occur for wind stress in a nearly alongshelf direction. For an alongshelf stress, the coastal sea level gains have a similar spatial structure to, and are of the same order of magnitude as, those estimated from observations by Noble and Butman (1979) and Thompson (1986, T2), although there is factor of two discrepancy between Noble and Butman's (1979) and Thompson's (T2) gains. We suggest that this discrepancy arises primarily from Noble and Butman's (1979) use of coastal wind observations and from their restriction to a relatively high frequency range and hence conclude that Thompson's (T2) observations are more appropriate for comparison with the present model predictions.

The present model also reproduces the qualitative features of several flows in the region. In particular, the predicted current gains are qualitatively consistent with the observational gains found by Smith (1986) for southwestern Nova Scotia and with those found by Noble et al. (1983) for Georges Bank. The large transports predicted for Northeast Channel are in the same sense (in relation to the wind stress and sea level changes in the GOM) and of the same order of magnitude as those observed by Ramp et al. (1986), and the flows in Georges and Jordan Basins are similar to those described by Brooks (1985). Nevertheless, it appears that final confirmation of the degree to which a barotropic model such as that used here can account for the current response of the GOM and adjacent regions to surface wind stress must await further analysis of observations and/or the inclusion of baroclinic effects in the model dynamics.

Acknowledgments. We are grateful to Dr. Keith Thompson of Dalhousie University for valuable discussion and for making the results of his sea-level analysis available to us, including revised gains calculated using regionwide wind stress. We also thank an anonymous reviewer for several helpful comments.

REFERENCES

Beardsley, R. C., and W. C. Boicourt, 1981: On estuarine and continental-shelf circulation in the Middle Atlantic Bight. *Evolution of Physical Oceanography,* B. A. Warren and C. Wunsch, Eds., The MIT Press, 233 pp.

——, and D. B. Haidvogel, 1981: Model studies of the wind-driven transient circulation in the Middle Atlantic Bight. Part I: Adiabatic boundary conditions. *J. Phys. Oceanogr.,* **11,** 355–375.

——, D. C. Chapman, K. H. Brink, S. R. Ramp and R. Schlitz, 1985: The Nantucket Shoals Flux Experiment (NFSE79). Part 1: A basic description of the current and temperature variability. *J. Phys. Oceanogr.,* **6,** 713–748.

Bigelow, H. B., 1927: Physical oceanography of the Gulf of Maine. *Bull. U.S. Bur. Fish.,* **40,** 511–1027.

Brink, K. H., 1983: Low-frequency free wave and wind-driven motions over a submarine bank. *J. Phys. Oceanogr.,* **13,** 103–116.

Brooks, D. A., 1985: Vernal circulation in the Gulf of Maine. *J. Geophys. Res.,* **90,** 4687–4705.

Butman, B., R. C. Beardsley, B. Magnell, D. Frye, J. A. Vermersch, R. Schlitz, R. Limeburner, W. R. Wright and M. A. Noble, 1982: Recent observations of the mean circulation on Georges Bank. *J. Phys. Oceanogr.,* **12,** 569–591.

——, J. W. Loder and R. C. Beardsley, 1986: The seasonal mean circulation on Georges Bank: Observation and theory. *Georges Bank,* R. H. Backus, Ed., The MIT Press (in press).

Csanady, G. T., 1974: Barotropic currents over the continental shelf. *J. Phys. Oceanogr.,* **4,** 357–371.

——, 1976: Mean circulation in shallow seas. *J. Geophys. Res.,* **81,** 5389–5399.

——, 1978: The arrested topographic wave. *J. Phys. Oceanogr.,* **8,** 47–62.

——, 1979: The pressure field along the western margin of the North Atlantic. *J. Geophys. Res.,* **84,** 4905–4913.

——, 1980: Longshore pressure gradients caused by offshore wind. *J. Geophys. Res.,* **85,** 1076–1084.

——, 1981: Shelf circulation cells. *Phil. Trans. Roy. Soc. London,* **A302,** 515–530.

Drinkwater, K., B. Petrie and W. H. Sutcliffe, Jr., 1979: Seasonal geostrophic transports along the Scotian Shelf. *Estuarine and Coastal Mar. Sci.,* **9,** 17–27.

Garrett, C., 1974: Normal modes of the Bay of Fundy and Gulf of Maine. *Can. J. Earth Sci.,* **11,** 549–556.

Greenberg, D. A., 1979: A numerical model investigation of tidal phenomena in the Bay of Fundy and Gulf of Maine. *Mar. Geodesy,* **2,** 161–187.

——, 1983: Modeling the mean barotropic circulation in the Bay of Fundy and Gulf of Maine. *J. Phys. Oceanogr.,* **13,** 886–904.

Hayashi, T., D. A. Greenberg and C. J. R. Garrett, 1986: Open boundary conditions for numerical models of shelf sea circulation. *Contin. Shelf Res.,* **5,** 487–497.

Heaps, N. S., 1978: Linearized vertically-integrated equations for residual circulation coastal seas. *Dtsch. Hydrogr. Z.,* **31,** 147–169.

Isaji, T., M. L. Spaulding and J. C. Swanson, 1982: A three-dimensional hydrodynamic model of wind and tidally-induced flows on Georges Bank. Interpretation of the Physical Oceanography of Georges Bank, Appendix A, EG&G Environmental Consultants, Waltham, MA, Final Rep. to U.S. Dept. of Interior, 901 pp.

Loder, J. W., 1980: Topographic rectification of tidal currents on the sides of Georges Bank. *J. Phys. Oceanogr.,* **10,** 1400–1416.

——, and D. G. Wright, 1985: Tidal rectification and frontal circulation on the sides of Georges Bank. *J. Mar. Res.,* **43,** 581–604.

Noble, M., and B. Butman, 1979: Low-frequency wind-induced sea level oscillations along the east coast of North America. *J. Geophys. Res.,* **84,** 3227–3236.

——, —— and E. Williams, 1983: On the longshelf structure and dynamics of subtidal currents on the eastern United States continental shelf. *J. Phys. Oceanogr.,* **13,** 2125–2147.

——, —— and M. Wimbush, 1985: Wind-current coupling on the southern flank of Georges Bank: Variation with season and frequency. *J. Phys. Oceanogr.,* **15,** 604–620.

Ramp, S. R., R. J. Schlitz and W. R. Wright, 1986: The deep flow through the Northeast Channel, Gulf of Maine. *J. Phys. Oceanogr.*, **15,** 1790–1808.

Sandstrom, H., 1980: On the wind-induced sea level changes on the Scotian Shelf. *J. Geophys. Res.*, **85,** 461–468.

Saunders, P. M., 1977: Wind stress on the ocean over the eastern continental shelf of North American. *J. Phys. Oceanogr.*, **7,** 555–566.

Shaw, P. T., 1982: The dynamics of mean circulation on the continental shelf. Ph.D. Thesis, Massachusetts Institute of Technology/Woods Hole Oceanographic Institution, WHOI Ref. 82-1, 226 pp.

Smith, P. C., 1983: The mean and seasonal circulation off southwest Nova Scotia. *J. Phys. Oceanogr.*, **13,** 1034–1054.

——, 1986: The wind-driven circulation off southwest Nova Scotia. (in preparation).

——, B. Petrie and C. R. Mann, 1978: Circulation, variability, and dynamics of the Scotian Shelf and Slope. *J. Fish. Res. Board Can.*, **35,** 1067–1083.

Thompson, K. R., 1986: North Atlantic sea level and circulation. *Geophys. J. Roy. Astron. Soc.* (in press).

——, and M. G. Hazen, 1983: Interseasonal changes of wind stress and Ekman upwelling: North Atlantic, 1950–80. Can. Tech. Rep. Fish. Aquat. Sci., No. 1214, 175 pp.

Wang, D. P., 1982: Effects of continental slope on the mean shelf circulation. *J. Phys. Oceanogr.*, **12,** 1524–1526.

Winant, C. D., 1979: Comments on "The arrested topographic wave." *J. Phys. Oceanogr.*, **9,** 1042–1043.

Wright, D. G., and K. R. Thompson, 1983: Time-averaged forms of the nonlinear stress law. *J. Phys. Oceanogr.*, **13,** 341–345.